Defects in hexagonal-AlN sheets by first-principles calculations

E. F. de Almeida Junior, F. de Brito Mota, C. M. C. de Castilho,
Anelia Kakanakova-Gueorguie and Gueorgui Kostov Gueorguiev

Original Publication:

E. F. de Almeida Junior, F. de Brito Mota, C. M. C. de Castilho, Anelia Kakanakova-Gueorguie and Gueorgui Kostov Gueorguiev, Defects in hexagonal-AlN sheets by first-principles calculations, 2012, European Physical Journal B: Condensed Matter Physics, (85), 1.
http://dx.doi.org/10.1140/epjb/e2011-20538-6

Defects in hexagonal-AlN sheets by first-principles calculations

Edward F. de Almeida Junior[1], Fernando de B. Mota[1], Caio M. C. de Castilho[1,2], A. Kakanakova-Georgieva[3], G. K. Gueorguiev[3]

[1] Grupo de Física de Superfícies e Materiais, Instituto de Física, Universidade Federal da Bahia, Campus Universitário da Federação, Rua Barão de Jeremoabo s/n, 40170-115 Salvador, Bahia, Brazil.
[2] Instituto Nacional de Ciência e Tecnologia em Energia e Ambiente (CIENAM) INCT-E&A, Universidade Federal da Bahia, Salvador, Bahia, Brazil.
[3] Department of Physics, Chemistry and Biology, IFM, Linköping University, SE 581 83 Linköping, Sweden.

Corresponding author: Email: edward@ufba.br

Abstract. Theoretical calculations focused on the stability of an infinite hexagonal AlN (h-AlN) sheet and its structural and electronic properties were carried out within the framework of DFT at the GGA-PBE level of theory. For the simulations, an h-AlN sheet model system consisting in 96 atoms per super-cell has been adopted. For h-AlN, we predict a lattice parameter of 1.82 Å and an indirect gap of 2.81 eV as well as a cohesive energy which is by 6% lower than that of the bulk (wurtzite) AlN which can be seen as a qualitative indication for synthesizability of individual h-AlN sheets. Besides the study of a perfect h-AlN sheet also the most typical defects, namely, vacancies, anti-site defects and impurities were also explored. The formation energies for these defects were calculated together with the total density of states and the corresponding projected states were also evaluated. The charge density in the region of the defects was also addressed. Energetically, the anti-site defects are the most costly, while the impurity defects are the most favorable, especially so for the defects arising from Si impurities. Defects such as nitrogen vacancies and Si impurities lead to a breaking of the planar shape of the h-AlN sheet and in some cases to formation of new bonds. The defects significantly change the band structure in the vicinity of the Fermi level in comparison to the band structure of the perfect h-AlN which can be used for deliberately tailoring the electronic properties of individual h-AlN sheets.

1. Introduction

The intense research dedicated to graphene generally triggered exploration into other two-dimensional (2D) hexagonal networks including h-BN [1, 2] which is considered of particular interest as a topological insulator [3]. Recently, 2D nanosheets of BN have been exfoliated, which is a prerequisite for developing the full potential of h-BN in applications ranging from electronics to energy storage [4].
Stability issues as well as electronic properties of 2D hexagonal sheets of other III-Nitrides, including h-AlN, are becoming a "hot" research topic, which can expand the range of possible applications of III-Nitrides and open new perspectives for miniaturization in engineering functional nano-devices and interconnects. Bulk AlN crystallizes in the wurtzite structure, space group P63mc, consisting in two interpenetrating hexagonal, close-packed lattices, thus being implicitly related to hexagonal networks.
AlN can be furnished as crystal boules and related sliced wafers [5], thick (~ 1-2 μm) individual epitaxial layers [6,7], and thin (~ 15 nm) barriers in AlN-based multiple quantum wells [8] developed for better carrier confinement and efficient light emission from semiconductor structures. The development of AlN constitutes the development of energy-efficient, reliable, and long-lifetime deep-UV light emitting diodes intended for applications in sustainable water/air purification and biomedical systems [9, 10].
Further, device applications of AlN as an optoelectronic and field-emission material could largely benefit from the accomplishment of crystallographically perfect low-dimensional objects such as AlN nanowires. AlN nano-wires [11, 12] and AlN nanoribbons [13] have been fabricated and characterized, while computational studies identify AlN nanowires/tubes as a prospective hydrogen storage media [14].
The h-AlN sheet considered in this work represents a prospective low-dimensional object with specific properties for which we perform first-principles calculations.
The bulk AlN which is a semiconductor with a wide gap (6.28 eV) exhibiting a *wurtzite* (wz) structure (with lattice parameters: a = 3.11 Å, c = 4.98 Å, c/a = 1.60) [15, 16, 17]. We find that the most stable 2D AlN network is the perfect infinite hexagonal-AlN sheet. We investigate the stability of this perfect h-AlN sheet and its structural and electronic properties.
We find that a perfect h-AlN sheet is only 6% less stable than bulk wz-AlN. We also study the energetics of typical defects in the h-AlN network such as vacancies, anti-sites and impurities together with their implications on the electronic properties of the h-AlN sheet.

2. Computational details

The framework adopted for the present calculations is DFT within its Generalized Gradient Approximation (GGA) with spin-polarization as implemented in the SIESTA code [18]. Norm-conservative Troullier-Martins pseudopotentials [19] in the Kleinmann-Bylander factorized form [20] and a double-ζ basis set, with spin-polarized functions (DZP) were employed. The adopted energy shift for determining the confining radii of

the pseudo-atomic orbitals is 0.10 eV. The grid in real space, used for obtaining the Hamiltonian matrix elements, employed a mesh cut off of 200 Ry.
An optimized h-AlN atomic sheet containing 96 atoms was simulated by adopting a planar unit cell with dimensions of 21.9 Å by 18.9 Å. Such size for the supercell ensures that when considering multiple point defects they will be sufficiently isolated from each other, thus avoiding defect-defect interactions. The relaxation criterion applied to the considered geometries demands residual Hellmann - Feynman forces weaker than 0.01 eV/Å.
The comparative analysis of structures with defects was always carried out relatively to an ideal (non-defective) layer. Similar to previous calculations for an h-BN layer [21], the investigated model systems have either an N or an Al-rich environment, depending on the atomic reservoir specifically employed.
The usual phase of constituent Nitrogen is gaseous (chemical potential μ_N) while the usual phase for constituent Al is solid (chemical potential for FCC Al μ_{Al}). The chemical potential for an AlN pair μ_{AlN} in an infinite AlN sheet is then restricted by the thermodynamic constraint:

$$\mu_{AlN} = \mu_N + \mu_{Al} \tag{1}$$

A similar procedure can be applied with respect to different impurities due to different chemical species other than the ones constituting the perfect layer.
Three different kinds of point defects in an AlN layer are considered:

i) a **vacancy** at an N place in the layers' network (V_N);

ii) an **anti-site defect, i.e.,** when at an N site there is an Al atom (N_{Al}), or vice-versa (Al_N);

iii) a **substitutional defect** - when an atom of a chemical element different from both N and Al occupies an N or Al site in the network (e.g., C atom at Al site is referred to as "C_{Al}", a Si atom at an N site as "Si_N", respectively);

The defect formation energy E_{form} corresponding to an anti-site or a substitutional defect X_Y, where the atom X occupies the site of the atom Y is given by the expression:

$$E_{form}[X_Y] = E_{tot}(h - AlN + X_Y) - E_{tot}(h - AlN) - \mu_X + \mu_Y \tag{2}$$

The defect formation energy E_{form} for a vacancy defect V_X, is then trivially defined by:

$$E_{form}[V_X] = E_{tot}(h - AlN + V_X) - E_{tot}(h - AlN) + \mu_X \tag{3}$$

In both expressions (2) and (3), E_{tot} (h-AlN+X_y) and E_{tot} (h-AlN+V_x), are calculated the total energy of the h-AlN layer with a defect, while E_{tot} (h-AlN) is the total energy of an ideal h-AlN sheet. For the determination of the chemical potentials μ_X and μ_Y, with X corresponding to N and Y to Al, μ_N (-321.51eV) is obtained from the nitrogen in the gas phase, while for μ_{Al} (-165.03 eV) a metallic aluminium phase is used as reservoir for Al-rich environment, the constraint express by equations (1) with μ_{AlN} (-484.88 eV). When

differences of energies are considered the reference energy value E_{tot} (h-AlN) is ascribed to 0 eV.
For evaluating the stability of an AlN model system, we also use the cohesive energy per atom $E_{coh/at}$ defined as follows:

$$E_{coh/at} = \left[E_{tot} - (n_N E_N + n_{Al} E_{Al})\right]/(n_N + n_{Al}) \quad (4)$$

where E_{tot} is the total energy of the model system, n_N and n_{Al} are the numbers of N and Al atoms per unit-cell, and E_N and E_{Al} are the energies of the isolated N and Al species, respectively.
In order to test the validity of the level of theory used for investigating h-AlN, we have also simulated the bulk AlN in its best studied wurtzite allotrope (wz-AlN). For the lattice parameter of wz-AlN we obtained 3.10 Å (to be compared to the experimental value of 3.11 Å [15]), while for its band gap the calculated value is 4.44 eV (similar to the values discussed in Ref. 22, and expectedly underestimating the experimental value of the wz-AlN band gap of 6.28 eV).

3. Results and discussions

3.1. Perfect infinite h-AlN sheet

The h-AlN sheet which underwent an optimization procedure is shown in the Fig. 1. The optimized Al-N bond length is 1.82 Å in good agreement with works by others [23, 24, 25] in which the authors, in contrast to our fully periodic network, have adopted periodic boundary conditions in one direction only passivating the remaining dangling bonds by H atoms.
The calculated value for the cohesive energy per atom (Eq. 4) for an infinite h-AlN sheet is -5.03 eV. For bulk wz-AlN and at the same level of theory, we obtain for $E_{coh/at}$ the value of -5.36 eV, emphasizing that the perfect infinite h-AlN sheet possesses a cohesive energy by only 6% lower than the bulk wz-AlN which can be seen as a qualitative hint to the synthesizability of individual h-AlN sheets.
The orbitals in h-AlN exhibit a $\boldsymbol{sp^2}$-hybridization. Since the Al atoms possess three valence electrons and the N atoms possess five valence electrons, two electrons per every N atom form a lone pair distributed perpendicularly to the plane of the sheet.
The Fig. 2 displays the total and projected spin-up and spin-down density of states (DOS) for the h-AlN. Since both densities of states are symmetric, the total spin is 0. In the energy region of about -20 eV, a major contribution to DOS comes from the ***s***-orbitals of the N atoms. In the region of band energies between -12 and -5.5 eV, the major contribution to the DOS comes from the ***p***-orbitals of the N atoms. In this energy range, the contribution of the Al ***p***-orbitals is more pronounced at about -8.0 eV. The contribution to the top of the valence band comes mostly from the N lone pairs. Above the Fermi level, there is a predominance of ***p***-orbitals of Al atoms. Thus, the sheet exhibits a well-defined $\boldsymbol{p_z}$ character added to its $\boldsymbol{sp^2}$ hybridization.
The band structure of an optimized infinite perfect h-AlN exhibits an indirect band gap of 2.81 eV defining the h-AlN as a wide gap semiconductor similarly to bulk AlN.

3.2. Defects incorporated in an h-AlN sheet

3.2.1. Vacancies

As any other material system, the electronic properties of the h-AlN sheet can change significantly by the presence of defects. If these defects can be controllably introduced, this property can be used in order to tailor physical properties.
To address vacancies and anti-sites, such defects were introduced, always at a rate of only one defect per unit-cell, and subsequently the model system underwent a geometry optimization. Figs. 3a and 3b display optimized h-AlN sheets incorporating the vacanies V_{Al} and V_N, respectively. As seen from Fig. 3a, for V_{Al}, the surrounding N atoms are not significantly displaced from their original positions, the distances between them, in the immediate vicinity of the Al vacancy, being 3.16 Å, 3.13 Å and 3.19 Å. Such distances are close to the distances between closest N neighbors in a perfect, unperturbed by a vacancy, h-AlN sheet. A very similar behavior is observed in an h-BN sheet incorporating a boron vacancy (V_B) [21, 26]. The presence of a V_{Al} vacancy in the h-AlN sheet generates three dangling bonds, which leads to a total spin value of S = 3/2.
In contrast to V_{Al}, in the case of V_N (Fig. 3b), the surrounding Al atoms are more significantly displaced from their equilibrium positions in the perfect h-AlN, with the optimized distances between them being now 2.84 Å, 3.13 Å and 3.15 Å. These different Al-Al distances in the vicinity of a V_N result in only one chemical Al-Al bond, corresponding to 2.84 Å distance. The other Al atom does not form a chemical bond. They also shift by 0.44 Å out of the h-AlN sheet plane. This bonding situation explains the calculated total spin value of S = 1/2, i.e., one unpaired electron associated with the V_N.
From the above discussion, it can be seen that the incorporation of the vacancies V_N and V_{Al} in a h-AlN sheet leads to an imbalance in the spin distribution, with different values for the total spin for V_N and V_{Al}. Such imbalance is usually associated with the Jahn-Teller effect [27] and can lead to more (V_N) or much less significant local structural distortion (V_{Al}).
In Fig. 4a, the projected DOS corresponding to V_{Al}, is shown. The ***s***-orbitals associated with the N atoms in vicinity of the V_{Al} appear in the energy region of - 18 eV while their ***p***-states can be identified as close to the Fermi level. No significant reconstruction in the bonding scheme happens around a V_{Al}. Consistent with this picture is the N-atoms $\boldsymbol{sp^2}$ dangling bonds charge distribution in the vicinity of a V_{Al} as illustrated in Fig. 5a.
The considerable structural reconstruction happening around a V_N is reflected in corresponding changes in the projected DOS (Fig. 4b). The V_N introduces two states associated with the Al ***p***-orbitals, one above and one below the Fermi level, with corresponding charge distribution in the vicinity of the V_N, as illustrated in Fig. 5b.
The formation energies for V_{Al} and V_N in both Al-rich and N-rich environments are listed in Table 1. As seen from Table 1, the V_N has stability advantage compared to V_{Al}. This advantage is present in both N and Al rich environments and is due to new chemical Al-Al bond in the system incorporating V_N after optimization of its geometry.

3.2.2. Anti-site defects

We obtain marked differences between the two anti-site defects in h-AlN. In the case of N_{Al}, the substituting N atom bonds to two of its three neighbor N atoms, as illustrated in Fig. 3c. Thus, two dangling bonds remain. In the case of Al_N, the substituting Al atom forms nonsymmetrical bonds with all of the three neighbors Al atoms (Fig. 3d). In addition, the substituting Al atom is shifted out of the h-AlN sheet plane by the considerable value of 1.84 Å. Formation energies for N_{Al} and Al_N are presented in Table 1 reading, e.g., in Al-rich environment, 9.74 eV and 6.73 eV respectively. Unsurprisingly, these values show that Al_N and N_{Al} are between the most energetically expensive defects in h-AlN. This is explained by the creation of the energetically unfavorable condition, for a binary compound as the AlN, of homo-nuclear bonds which also leads to a considerable local distortion and, in the case of N_{Al}, to dangling bonds.
In Fig. 4c and 4d the projected DOS for N_{Al} and Al_N are displayed. In the case of N_{Al} and in comparison to the perfect h-AlN network, several new states (mostly associated with the ***p***-orbitals of N atoms) emerge, either for spin up and spin down. This leads to a spin polarized network with a total spin S = 1. In Fig. 5c, the spin excess associated with the dangling bonds due to a N_{Al} defect, is illustrated.
The Al_N defect does not introduce a spin imbalance, since there is a symmetric spin distribution between spins up and spin down, due to the lack of dangling bonds in this case. However, new states do appear when its DOS is compared to those of the perfect h-AlN. These symmetric new states appear in close vicinity (above and below) of the Fermi level (Fig. 3d).

3.2.3. Impurities

Following both the importance of substitutional impurities such as C [28] and Si [29] for the electronic and optical performance of bulk wz-AlN and the suitability of substitutional C and Si, for creating covalent bonds and not entirely disrupting the AlN network (in contrast to many other chemical elements, for example Fluorine, which would cause disruption of the h-AlN sheet), we have considered C and Si impurities in h-AlN.
The substitutional impurities due to C atom incorporation (C_{Al}, C_N) and Si atom incorporation (Si_{Al}, Si_N) in h-AlN are shown in Fig. 6a, b, c, and d, respectively. In Table 1 the corresponding formation energies for these impurities are listed. From the data in Table 1 a pattern emerges: the formation energy, which can be perceived as the energy cost for stabilizing the corresponding defect, is lower for C_{Al} in an N-rich environment and for C_N in an Al-rich medium. This pattern persists when Si impurities are incorporated in an h-AlN network, with Si_{Al} exhibiting a lower energy cost in an N-rich medium, and with Si_N being more easily formed in an Al-rich environment.
Considering the geometry changes due to impurity incorporation, we observe that the substitutional C atoms remain in the plane of the h-AlN network. In contrast, in the case of Si_{Al}, after optimization, the defect is shifted out of the h-AlN plane by 0.46 Å and, in the case of Si_N, the Si atom displacement out of the h-AlN plane is much more significant, reading 1.94 Å, a value comparable to the shift out of the h-AlN plane associated with the Al_N defect. However, the significant difference between Si_N and Al_N defects is that, see

Table 1, the Si_N defect is energetically more favorable and consequently more feasible to prevail.

The projected DOS for C_{Al} and C_N are displayed in Fig. 7a, and b, while the corresponding charge distributions associated with the spin excess in the vicinity of these defects are shown in Figs. 5d, and e. In the case of C_{Al}, several new states due to the C atom incorporation emerge. They are quasi-symmetric for spins up and spin down in the case of C_{Al} (Fig. 5d), and non-symmetric for C_N (Fig. 5e). In close vicinity below the Fermi level, there is a ***p***-state due to the C atom impurity. This state exhibits features similar to the ones of a shallow donor impurity. Fig. 5d illustrates what is a well delocalized orbital associated to C_{Al}. Due to this orbital delocalization, during the model system relaxation it was necessary to adopt a unit-cell containing 384 atoms (instead of 96 for most of our calculations) in order to avoid mutual interaction between defects located in neighboring unit-cells. An opposite behavior, as compared with the C_{Al}, was identified for C_N (Fig. 5e). As a result of an odd number of electrons associated with the C_N defect, an imbalance of spins emerges. However, the state associated to this spin excess is situated inside the valence band, together with an empty state just above the Fermi level. Thus, in sharp contrast to the C_{Al} defect (Fig. 5d), C_N is associated with a well localized state. A trivial common feature for both defects, C_{Al} and C_N, since they imply the same impurity species, is that in both cases the total spin is 1/2.

In the case Si_{Al}, the atoms remain in the plane, and the Si atom has a quasi-symmetric behavior with respect to the neighboring N atoms (Fig. 6c). For Si_N the Si atom suffers a large plane displacement of 1.94 Å, with its configuration being similar to the one of Al_N. (Fig. 6d)

The projected DOS for Si_{Al} and Si_N are illustrated in Fig. 7c, and d. Similarly to C_{Al} and C_N, also for Si_{Al} and Si_N there are spin imbalances corresponding to a total spin 1/2. As seen in Fig. 7c, for Si_{Al} as compared to perfect h-AlN, a Si-originated ***p***-orbital emerges in close vicinity below the Fermi level, in addition to another unoccupied orbital well above it, i.e., inside the conduction band. Fig. 7d illustrates the fact that the spin excess is associated with both the Si-originated ***p***-orbital and the lone pairs of the N atoms neighboring to Si_N.

Similarly to C_{Al}, for the correct description of the Si_{Al} defect, a larger supercell with 384 atoms was used. For Si_{Al}, additional ***p***-orbitals emerge, as shown in Fig. 5f. For Si_N, as expected, the charge distribution associated with the spin is much more localized (Fig. 5g).

A general feature of the impurity defects in h-AlN is their lower energy cost (as judged by the E_{form}, see Table 1) when compared to vacancies and anti-site effects. The increased feasibility of substitutional defects in h-AlN can have both a positive (when searching for tailoring the electronic properties of a model system) and negative (due to unavoidable impurities during material growth) impact on possible applications for h-AlN.

4. Conclusions

The structural and electronic properties of an infinite individual h-AlN sheet were addressed by DFT calculations together with the implications for its network of selected defects – vacancies, anti-sites as well as C and Si impurities. A perfect h-AlN sheet exhibits an Al-N bond length of 1.82 Å and a band-gap of 2.81 eV which classifies it as a

wide-band gap semiconductor. The cohesive energy per atom for an infinite h-AlN sheet is -5.03 eV which is only by 6%, in absolute value, lower than the cohesive energy of bulk wz-AlN. Among all the defects studied, the anti-site defects which introduce homo-nuclear bonds are expectedly the least feasible, while the impurity defects are the most energetically favorable. This is especially so for the defects arising from a Si impurity (Si_{Al} and Si_N). In what concerns the expected defect prevalence during a hypothetic h-AlN synthesis as judged by energy cost and geometric criteria, the vacancies occupy an intermediate position between the anti-site defects and the impurities. Some defects such as V_N, Al_N, Si_{Al} and Si_N lead to a breaking of the planar shape of the h-AlN due to atomic species sticking out of the sheet plane, and in some cases to formation of new bonds.
The detailed picture of the density of states for an h-AlN sheets incorporating defects makes clear that the defects significantly change the DOS in the vicinity of the gap and the Fermi level in comparison to the DOS of the perfect h-AlN, which can be used for deliberately tailoring the electronic properties of individual h-AlN sheets.

5. **Acknowledgments**

The authors gratefully acknowledge support by STINT (Swedish Foundation for International Cooperation in Research and Higher Education) as well as by CAPES (Coordenação de Aperfeiçoamento de Pessoal de Nível Superior - Brazil), CNPq (Conselho Nacional de Desenvolvimento Científico e Tecnológico - Brazil), and Fundação de Amparo à Pesquisa do Estado da Bahia - FAPESB – Brazil. A.K-G. and G.K.G. acknowledge~~s~~ support by Swedish Research Council (VR). The National Supercomputer Center (NSC) in Linköping is acknowledged for providing high performance computing resources.

References

[1] K. S. Novoselov, D. Jiang, F. Schedin, T. J. Booth, V. V. Khotkevich, S. V. Morozov and A. K. Geim, PNAS **102,** 10451 (2005)
[2] M. Farahani, T. S. Ahmadi and A. Seif, J. Mol. Struc. **126,** 913 (2009)
[3] S. K. Mishra, S. Satpathy and O. Jepsen, J. Phys. Condens. Matter **9,** 461 (1997)
[4] J. N. Coleman *et al,* Science **331,** 568 (2011)
[5] D. Ehrentaut and Z. Sitar, MRS Bulletin **34,** 259 (2009)
[6] R. Dalmau, B. Moody, R. Schlesser, S. Mita, J. Xie, M. Feneberg, B. Neuschl, K. Thonke, R. Collazo, A. Rice, J. Tweedie and Z. Sitar, J. Electrochem. Soc. **158,** H530 (2011)
[7] A. Kakanakova-Georgieva, R. R. Ciechonski and U. Forsberg *et al,* Cryst. Growth & Design **9,** 880 (2009)
[8] T. Oto, R. G. Banal, K. Kataoka, M. Funato and Y. Kawakami, Nature Photonics **4.** 767 (2010)
[9] Y. Taniyasu, M. Kasu and T. Makimoto, Nature **441,** 325 (2006)
[10] A. Khan, K. Balakrishnan and T. Katona, Nature Photonics **2,** 77 (2008)
[11] O. Landré, V. Fellman, P. Jaffrennou, C. Bougerol, H. Renevier, A. Cros and B. Daudin, Appl. Phys. Lett. **96,** 061912 (2010)
[12] Z.-H. Yuan, S.-Q. Sun, Y. Q. Duan and D.-J. Wang, Nanoscale Res. Lett **4,** 1126 (2009)
[13] T. Xie, Y. Lin, G. Wu, X. Yuan, Z. Jiang, C. Ye, G.Meng, L. Zhang, Inorganic Chemistry Communications **7,** 545 (2004)
[14] Y. Li, Z. Zhou, P. Shen, S. B. Zhang and Z. Chen, Nanotechnology **20,** 215701 (2009)
[15] *Springer Handbook of Condensed Matter and Materials Data Springer Berlin-Heidelberg,* edited by W. Martienssen and G. Warlimont (2005)
[16] W.-G. Jung, S.-H. Jung, P. Kung and M. Razeghi, Nanotechnology **17,** 54 (2006)
[17] O. Ambacher, J. Phys. D: Appl. Phys. **31,** 2653 (1998)
[18] D. Sanchez-Portal, P. Ordejon, E. Artacho and J. M. Soler, Int. J. of Quantum Chem. **65,** 453 (1997)
[19] N. Troullier and J. L. Martins, Phys. Rev. B **43,** 1993 (1991)
[20] L. Kleinman and D. M. Bylander, Phys. Rev. Lett. **48,** 1425 (1982)
[21] S. Azevedo, J. Kaschny, C. M. C. de Castilho and F. B. Mota, Nanotechnology **18,** 495707 (2007)
[22] S. Loughin, R. H. French, W. Y. Ching, Y. N. Xu and G. A. Slack, Appl. Phys. Lett. **63,** 1182 (1993)
[23] Y. Wang and S.Shi, Solid State Comm. **150,** 1473 (2010)
[24] F.-L. Zheng, J.-M. Zhang, Y. Zhang and V. Ji, Physica B **405,** 3775 (2010)
[25] S. Hou, J. Zhang, Z. Shen, X. Zhao and Z. Xue, Physica E **27,** 45 (2005)
[26] S. Azevedo, J. Kaschny, C. M. C. de Castilho and F. B. Mota, Eur. Phys. J. B **67,** 507 (2009)
[27] R. F. Liu and C. Cheng, Phys. Rev B **76,** 014405 (2007)
[28] P. Boguslawski, E. L. Briggs and J. Bernholc, Appl. Phys. Lett. **69,** 233 (1996)
[29] E. Monroy, J. Zenneck, G. Cherkashinin et al, Appl. Phys. Lett. **88,** 071906 (2006)

Table 1. Formation energy (eV) for different defects incorporated in an infinite 2D h-AlN sheet. See main text for details.

Defect	N-rich	Al-rich
V_{Al}	7.79	9.45
V_N	4.44	2.78
N_{Al}	6.43	9.74
Al_N	10.04	6.73
C_{Al}	3.41	5.07
C_N	4.15	2.49
Si_{Al}	0.72	2.38
Si_N	4.79	3.13

Figure captions:

Fig.1. Portion of the unit cell of an h-AlN sheet.

Fig.2. Projected DOS for a perfect h-AlN.

Fig.3. Vacancies and anti-sites in an h-AlN: a) V_{Al}; b) V_N; c) N_{Al}; d) Al_N; Bond lengths in vicinity of each defect are shown in Å.

Fig.4. Projected DOS for: a) V_{Al}; b) V_N; c) N_{Al}; d) Al_N.

Fig.5. Charge distribution iso-surfaces associated to the spin excess emerging from the following defects incorporated in an h-AlN sheet: a) V_{Al}; b) V_N; c) N_{Al}; d) C_{Al}; e) C_N; f) Si_{Al}; and g) Si_N.

Fig.6. Substitutional impurities in h-AlN: a) C_{Al}; b) C_N; c) Si_{Al}; d) Si_N. Bond lengths in vicinity of each defect are shown in Å.

Fig.7. Projected DOS for an h-AlN sheet incorporating the following: a) C_{Al}, b) C_N; c) Si_{Al}; d) Si_N.

Figure 1

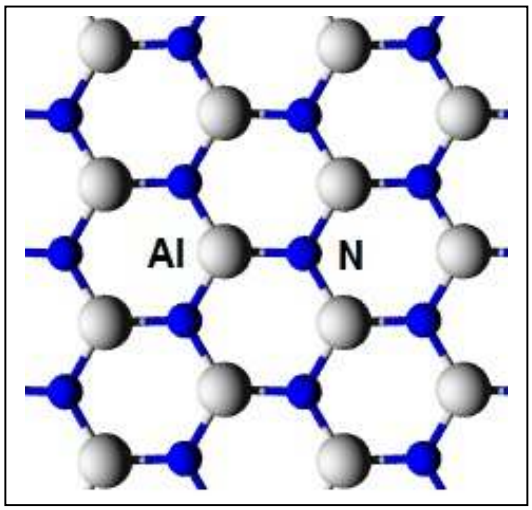

Figure 2

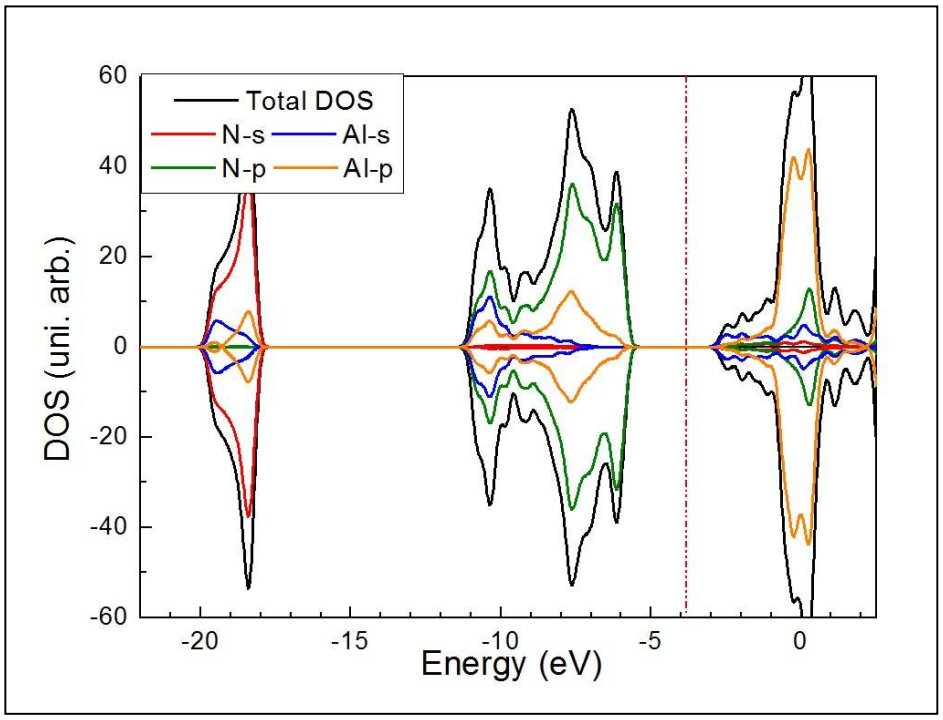

Figure 3

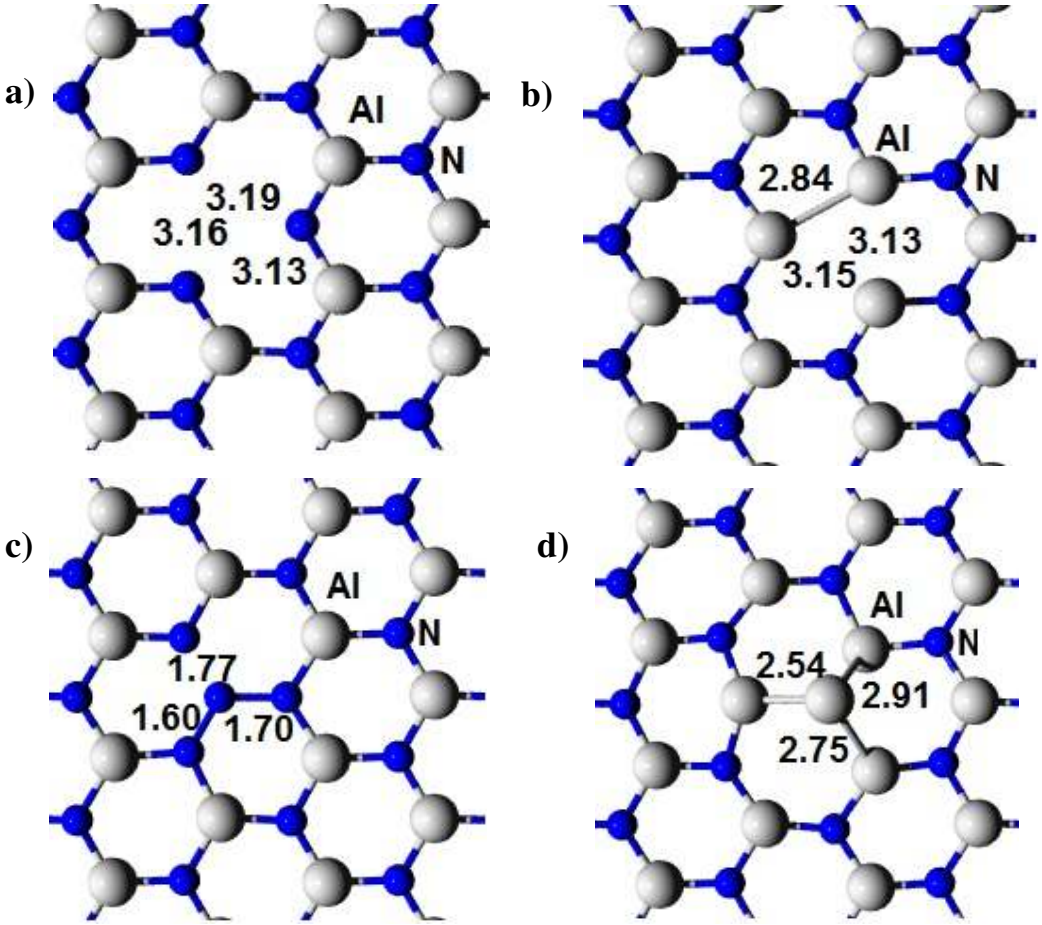
a)
Al
N
3.19
3.16
3.13
b)
Al
2.84
N
3.13
3.15
c)
Al
N
1.77
1.60
1.70
d)
Al
N
2.54
2.91
2.75

Figure 4

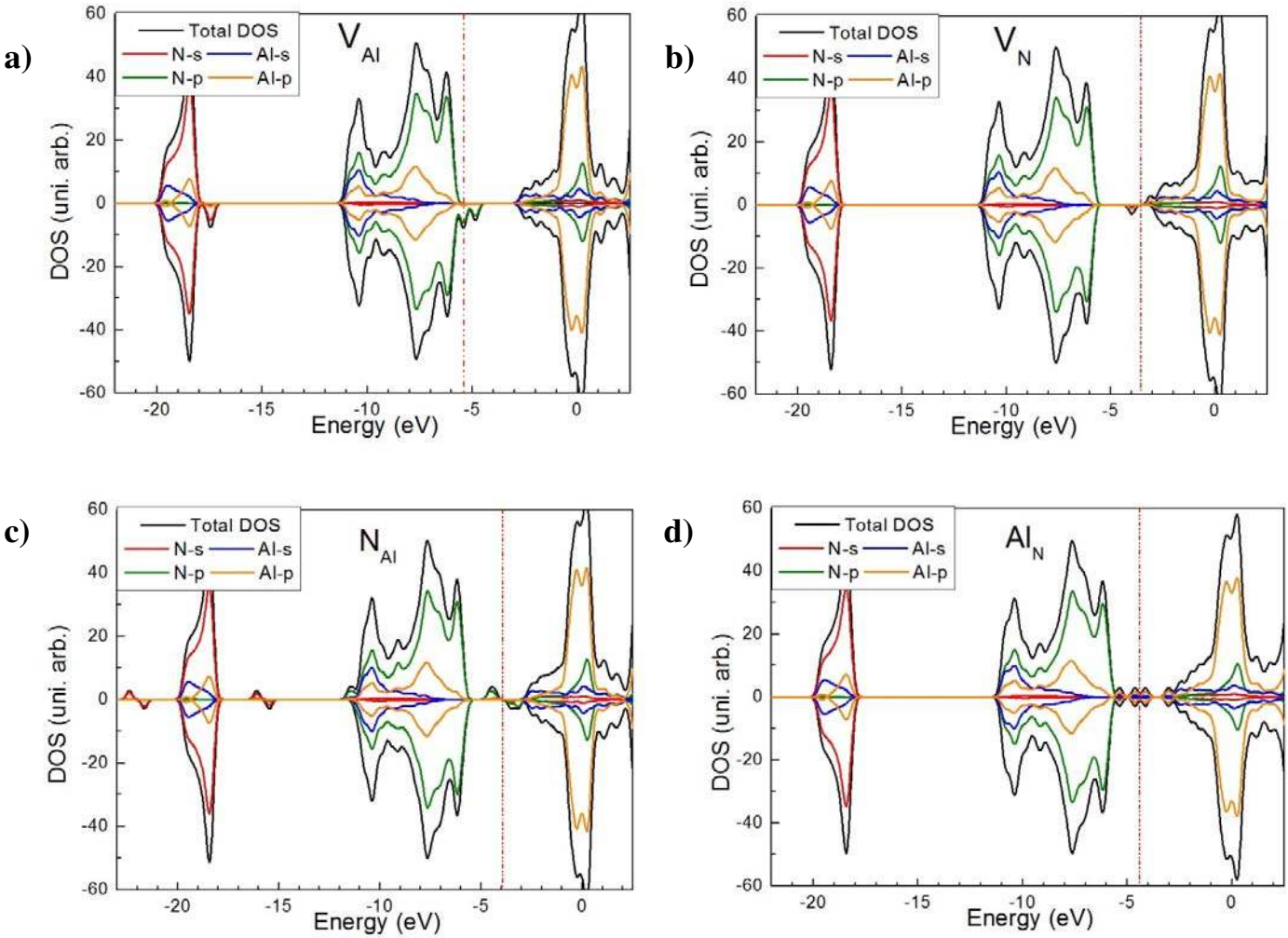
a)
Total DOS
N-s
Al-s
N-p
Al-p
V_{Al}
DOS (uni. arb.)
Energy (eV)
b)
V_N
c)
N_{Al}
d)
Al_N

Figure 5

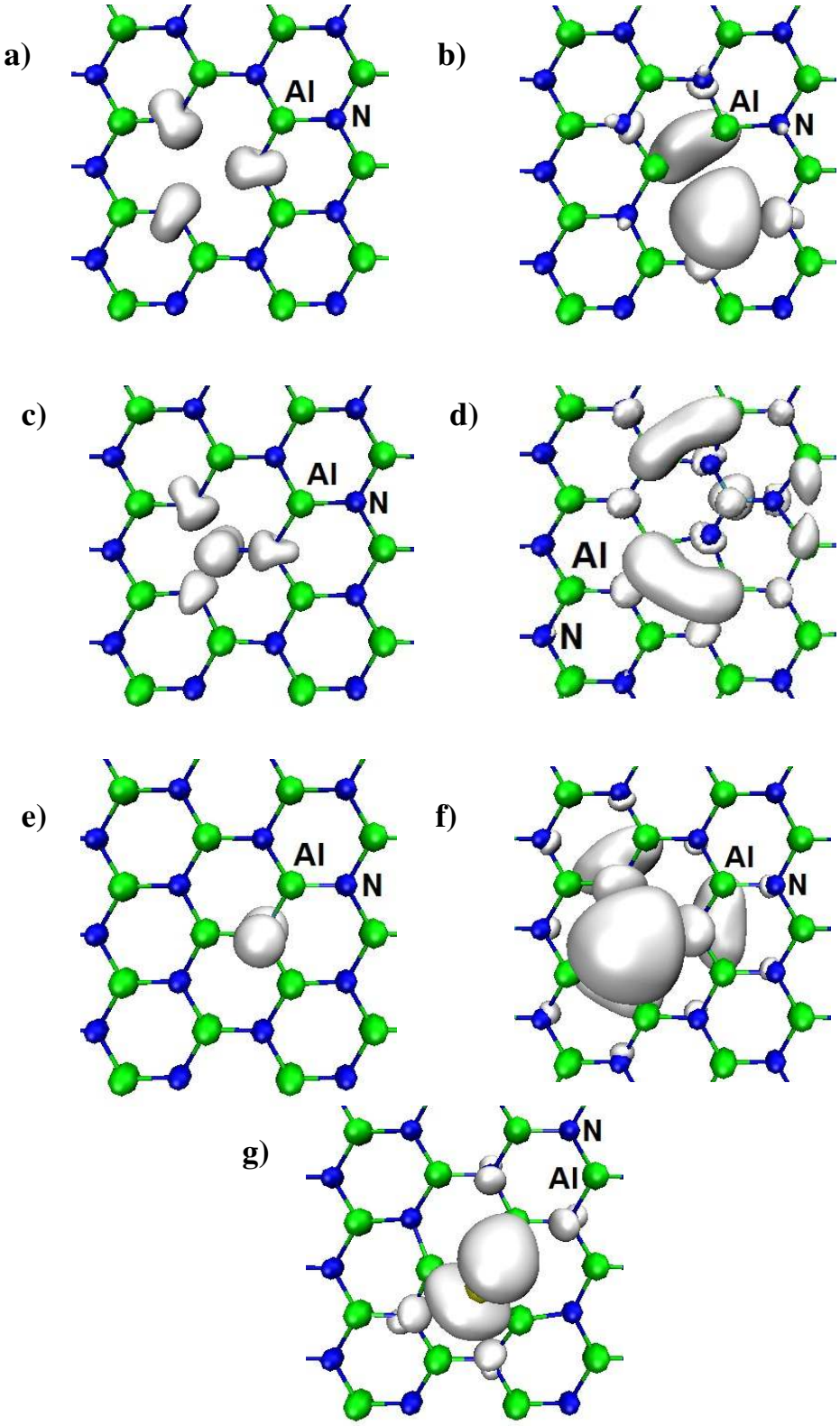

Figure 6

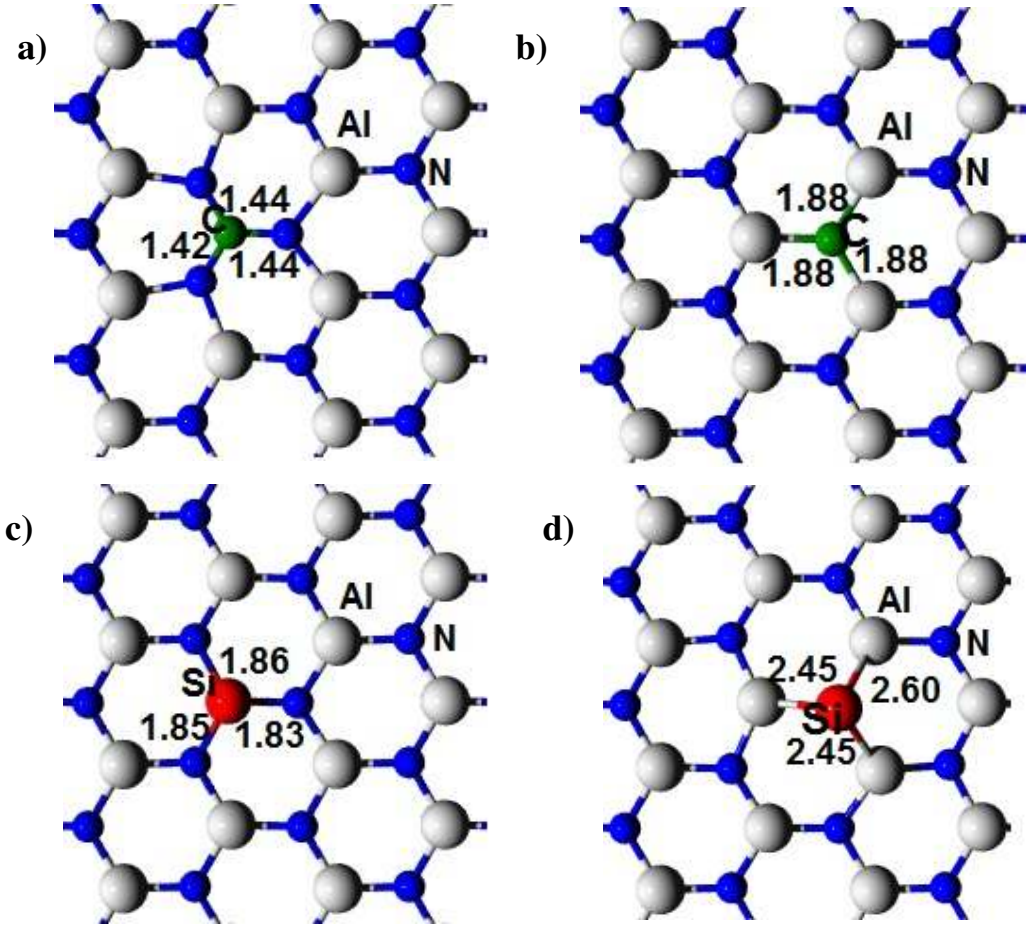
a)
Al
N
C
1.44
1.42
1.44
b)
Al
N
C
1.88
1.88
1.88
c)
Al
N
Si
1.86
1.85
1.83
d)
Al
N
Si
2.45
2.60
2.45

Figure 7

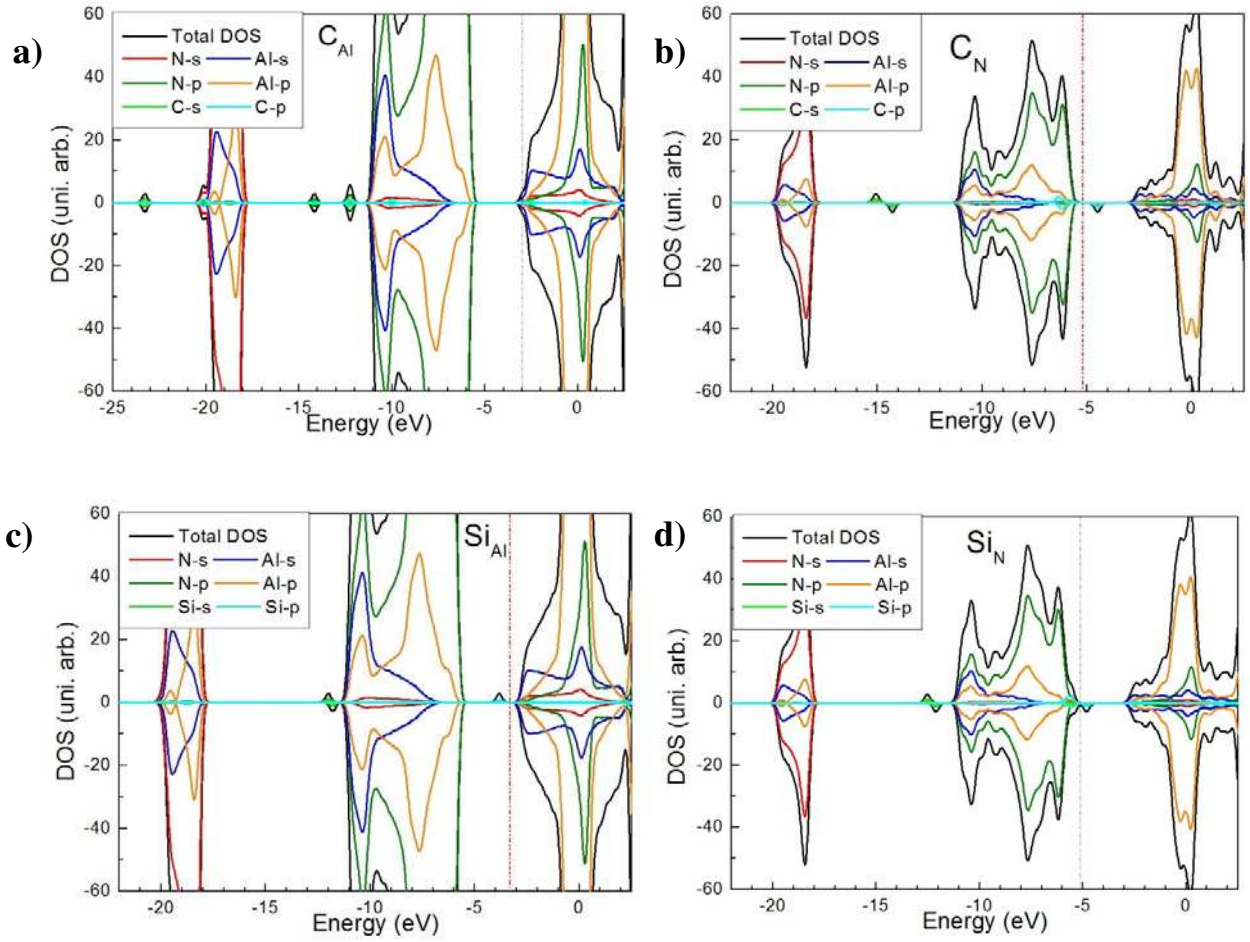
a)
Total DOS
N-s
Al-s
N-p
Al-p
C-s
C-p
C_{Al}
DOS (uni. arb.)
Energy (eV)
b)
C_N
c)
Si-s
Si-p
Si_{Al}
d)
Si_N